

LA-UR-14-21260

Approved for public release; distribution is unlimited.

Title: Development of Eulerian Code Modeling for ICF Experiments

Author(s): Bradley, Paul A.

Intended for: Report

Issued: 2014-02-27



Disclaimer:

Los Alamos National Laboratory, an affirmative action/equal opportunity employer, is operated by the Los Alamos National Security, LLC for the National Nuclear Security Administration of the U.S. Department of Energy under contract DE-AC52-06NA25396. By approving this article, the publisher recognizes that the U.S. Government retains nonexclusive, royalty-free license to publish or reproduce the published form of this contribution, or to allow others to do so, for U.S. Government purposes.

Los Alamos National Laboratory requests that the publisher identify this article as work performed under the auspices of the U.S. Department of Energy. Los Alamos National Laboratory strongly supports academic freedom and a researcher's right to publish; as an institution, however, the Laboratory does not endorse the viewpoint of a publication or guarantee its technical correctness.

Development of Eulerian Code Modeling for ICF Experiments

P. A. Bradley^{1,a}

¹*Los Alamos National Laboratory, Los Alamos, NM 87545, USA*

February 24, 2014 version by PAB LA-UR-14-0XXXX

a) Electronic mail: pbradley@lanl.gov

One of the most pressing unexplained phenomena standing in the way of ICF ignition is understanding mix and how it interacts with burn. Experiments were being designed and fielded as part of the Defect-Induced Mix Experiment (DIME) project to obtain data about the extent of material mix and how this mix influenced burn. Experiments on the Omega laser and National Ignition Facility (NIF) provided detailed data for comparison to the Eulerian code RAGE¹. The Omega experiments were able to resolve the mix and provide “proof of principle” support for subsequent NIF experiments, which were fielded from July 2012 through June 2013. The Omega shots were fired at least once per year between 2009 and 2012. RAGE was not originally designed to model inertial confinement fusion (ICF) implosions. It still lacks lasers, so the code has been validated using an energy source. To test RAGE, the simulation output is compared to data and by means of postprocessing tools that were developed. Here, the various postprocessing tools are described with illustrative examples.

I. Introduction

The Defect-Induced Mix Experiment (DIME) was developed in response to a request by NNSA to the labs to develop an experimental platform that would make use of ignition on the NIF to address physics issues. Here, we limit ourselves to the RAGE code¹ and the BHR-2² and BHR-3³ mix models. We emphasize that our experiments and results are general enough that they should be applicable to other codes and mix models, including the coming RAGE improvements to BHR and thermonuclear burn models. The experiments have changed somewhat in the last four years and now are designed to use multiple monochromatic imaging (MMI) spectra to image the hot mixed regions and use neutron imaging to see the burn region simultaneously in a capsule. RAGE was designed for radiation-hydrodynamic fluid simulations, so the needed physics for ICF and high-energy density (HED) physics is in the process of being implemented. In addition, we must develop postprocessing tools that will allow us to directly compare simulation output to data for quantitative analysis. In this paper, we focus our attention on the postprocessing tools and how we compare to diagnostic output. We refer the reader to papers by Magelssen et al.⁴, Bradley et al.⁵, Cobble et al.⁶ and Schmitt et al.⁷ for additional descriptions of the experiments along with their physics results and analysis.

II. The Experiments

We fielded experiments on two facilities. The first facility is Omega⁸ and the second is the National Ignition Facility (NIF)⁹. The Omega experiments use polystyrene (CH) plastic shells that range from 8.5 to 19 μm thick and outer diameters between 850 and 890 μm . The capsules have 5 atm of D₂ or DT gas in the center. The laser drive is a 1 ns

square pulse with drive energies of 23 kJ (60 beam drive) or 16 to 18 kJ (40 beam Polar Direct Drive = PDD). RAGE does not have lasers at this time, so we use an energy source in the outer portion of the shell (e.g, 7 μm thick for a 15 μm thick shell or 2 μm thick for an 8.5 μm thick shell). Previous data¹⁰ show that the capsules absorb about 60 to 65% of the incident laser energy. We vary the amount of energy in the source within the above range and the thickness of the source region to match the experimental bang time (time of peak neutron production). We fielded shots in 2009, 2010, 2011, and 2012. We have a variety of data from these shots, as listed in [Table 1](#). The diagnostics highlighted in red are unique to the NIF (see next paragraph). In the subsequent discussion, we will show illustrative comparisons, with an emphasis on comparisons that required development of postprocessing tools. We refer the reader to other papers produced by our group^{4,5,6,7} for detailed comparisons and physics analysis of these shots. We have also fielded four capsules on the NIF as part of our campaign, but will not report on those shots here as the diagnostics fielded so far on the NIF are similar to the Omega diagnostics.

Table 1: Diagnostics used for experiments and quantities that are constrained.

Diagnostic	Data Comparison	Quantity Constrained
Backlit images	Radius versus time	Zero-order hydro
Backlit images	Radius versus angle (P_2/P_0 , P_4/P_0)	Early time asymmetry
Self-emission images	Radius versus angle (P_2/P_0 , P_4/P_0)	Late time asymmetry
Streak spectra	Line emission spectra (spatial avg)	Burn-thru and mix
Multiple monochromatic images	Spatially resolved line emission	Spatial distribution of mixed material
Particle time-of-flight (PToF), gamma reaction history (GRH), or neutron time of flight (nToF)	Bang time (peak yield)	Bulk hydro
WRF, MRS, etc.	Secondary reaction yields	Fuel and shell pr
Neutron yield (DD, DT, TT)	Yield over mix	Burn/mix
Doppler broadened DD or DT peak	Burn averaged Tion	Bulk burn rate
#neutrons versus time	Burn width/burn history	Shock compression and effect on burn
Neutron imager	Neutron images	Spatial resolution of burn region
FFLEX	High energy x-rays from hot electrons	Hot electron preheat (hydro)

NOTE: entries in red are available only on the NIF

We started fielding experiments on the NIF in 2012. Again, we use polystyrene (CH) shells, but they are 2200 to 2300 μm in diameter and 40 to 42 μm thick. The gas fill has been 5 atm of deuterium, but we expect to use tritium in the near future. The laser drive has been \sim 650 to 700 kJ in a PDD configuration with a pulse length of 2.15 ns. As of January 2013, we have fielded four capsule implosions. We have also fielded two laser illuminated foil experiments that were part of our effort to commission a new multiple monochromatic imager¹¹ (MMI) for the NIF. Although the shot rate is lower on the NIF, it has several important advantages. First, the capsules are about 2.5 times bigger and this means we obtain more detailed images for a given diagnostic resolution than on Omega.

NIF is also more flexible in that we can field separated reactant capsules with CD shells and tritium gas. Also, we can make the capsules big enough and drive them hard enough that we expect to obtain high enough neutron yields to allow profitable use of the neutron imager and other diagnostics. This is crucial to our goal of obtaining simultaneous neutron images (image the burning region) and MMI images (see where hot mixed material is). This diagnostic information will tell us where material is mixed and how that mixed material is affecting the burn. Suitable variations in capsules will allow us to change the reactivity of a burning capsule in a controlled way and thus allow us to constrain whether the burning material is atomic (particle size much smaller than a neutron or charged particle mean free path) or chunk (particle size comparable to a mean free path) on a subgrid scale. Besides the diagnostics available on Omega, we have additional diagnostics for the NIF (highlighted in red in Table 1).

III. Diagnostic Comparisons

In this section, we illustrate comparisons of simulations with diagnostic results. We highlight places where we had to develop postprocessing tools to facilitate comparisons. In all cases, the simulation code is RAGE. We note that HYDRA¹² has been used extensively for ICF experiments, but our emphasis is to use an Eulerian code (RAGE)¹ for the experimental modeling. This allows us to follow complicated flows without rezoning, which may be affecting arbitrary-Lagrange-Eulerian (ALE) codes like HYDRA. In particular, improvements to the BHR mix model and the burn equations will

be available soon. We emphasize that the results shown here are not intended to be part of a final analysis. Those results are published elsewhere^{4,5,6,7}.

A. X-ray imaging diagnostics

We start our comparison with backlit images of the imploding capsules, with an example shown in Figure 1. The Large Format Camera¹³ can record up to 36 images in six rows of six images. The resolution is about 10 μm . The timing error is as small as 20 ps when the laser first illuminates the target and increases from one strip to the next, because one must make the assumption that images of equivalent radius on two different strips must have been taken at the same time. By bang time, the timing error can be +/- 75 ps. Radii are determined from multiple points and subjected to a least-squares analysis. The typical measurement error of the radius determination is 2 to 3 μm . In RAGE, we can create simulated backlit images based on the opacity of the materials in the shell. This procedure is used to create the simulated image in the right panel of Figure 1. We typically choose the 80% transmission contour to determine the radius, although the exact point is chosen to best conform with the experimental measurement. We show a comparison of radius versus time data against simulations in Figure 2. The typical mismatch between the data and a given simulation point is less than 20 μm , and when we compare a shot to a simulation designed to match it, the error is less than 10 μm for most points. In principle one can also use the density of and temperature of the mesh with opacity tables to create images for a given backlighter intensity and wavelength. In addition to backlit images, one can also use self-emission of the outer surface where the laser is being absorbed by the capsule to determine the capsule radius. This works well

when the laser is on, but after the laser turns off, the change in temperature profile makes a determination of the capsule outer radius ambiguous.

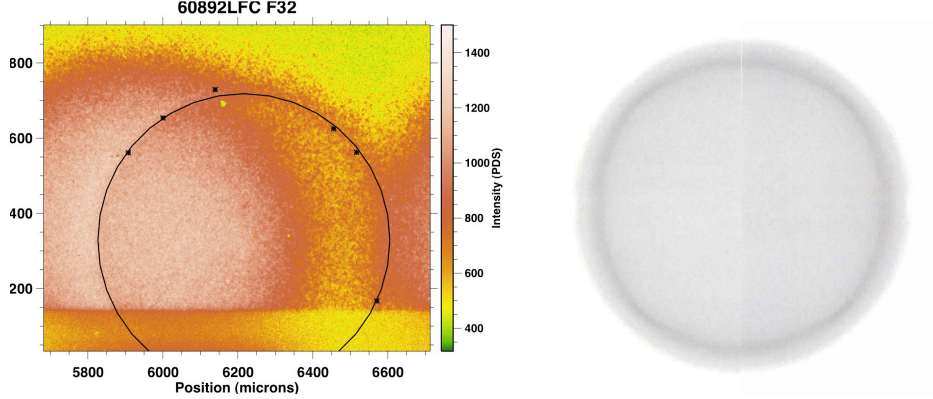


Figure 1: Backlit image for a PDD Omega shot in January 2011 (left panel). The black circle is a “best fit” to points around the outside of the capsule. The large orange region to the left is an image of the chlorine backscatterer foil. The right panel shows a simulated backlit image of the same capsule (the contrast was enhanced to make the contours visible).

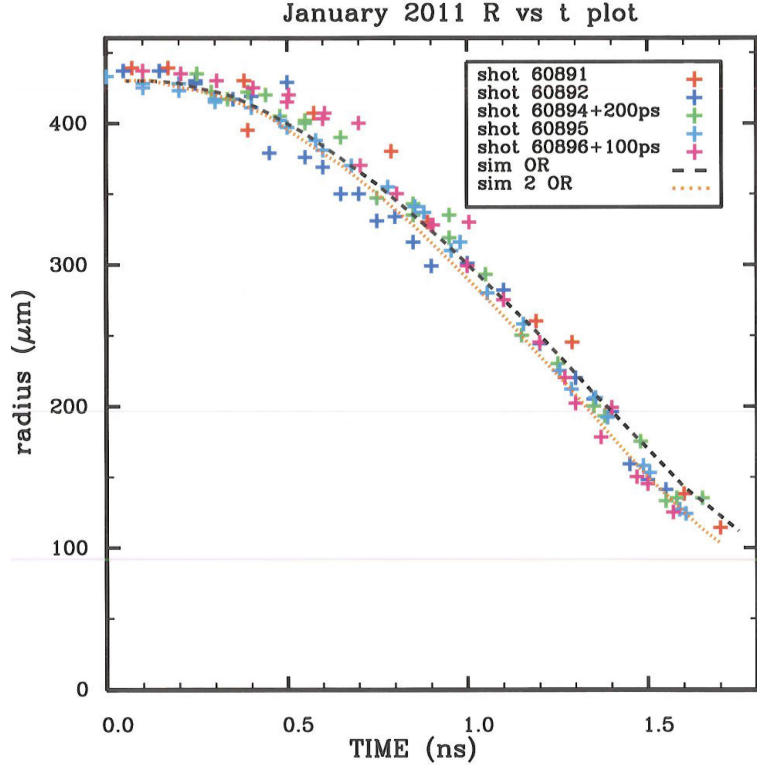


Figure 2: Radius versus time data for five shots in January 2011 (colored “+” signs) versus simulations (dashed lines). The simulation radii encompass the range of initial capsule radius, shell thickness, gas fill, and drive energy. The typical error between a simulation and the data is less than 20 μm .

Near bang time, the capsule compresses enough to reach temperatures of several keV, and becomes hot enough to self-emit. The x-rays cameras are timed to capture these images, as shown in Figure 3 for a representative PDD case. This image was taken at 1.56 ns (bang time is 1.77 ns) and the image is decidedly oblate ($P_2/P_0 \sim -0.25$). The synthetic image is obtained via postprocessing by treating the entire emitting core as a blackbody surrounded by a somewhat opaque shell. The diagnostic typically has a gate time of 60 to 80 ps, and we add up several synthetic images over this gate time to account for motion blur and changing core size. In the case of Figure 3, we replicate the data remarkably well, with both images having the same size of 60 by 40 μm . The backlit and self-emission images can also be analyzed to obtain asymmetry, which we typically express in terms of the Legendre moments P_2/P_0 and P_4/P_0 . Typically there is not much asymmetry in the early time images, but the self-emission images of the imploded core can show significant asymmetry.

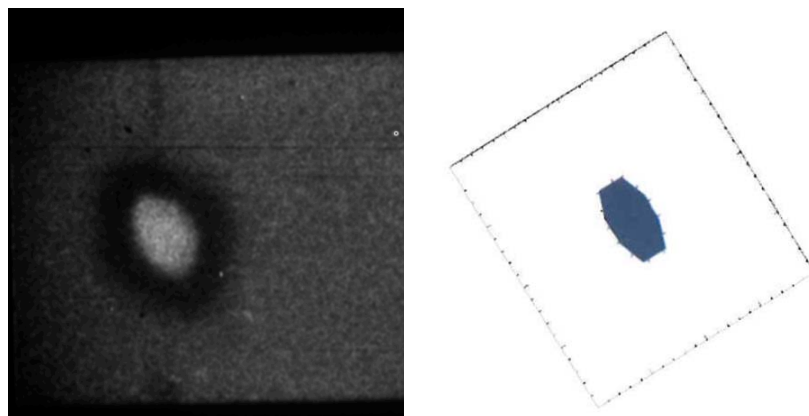


Figure 3: Self-emission image from shot 62801 at 1.56 ns (image is 60 x 40 μm across) in the left panel. A post-processed simulated image in the right panel and is the same size as the data. The capsule equator goes through the long axis of each image.

B. Neutron Yield and Neutron Spectra Diagnostics

The next set of diagnostics covers neutron yields. These include: the time of peak neutron yield (bang time), neutron yield, and burn history. The bang time provides information about the zero-order hydro of the implosion, the neutron yield is strongly affected by the mix, while the time-dependent neutron yield (burn history) can provide insight on how much of the yield from the initial shock hitting the center versus recompression of the outgoing shock by the incoming shell. RAGE computes the neutron yield from DD, DT, and TT reactions among others, as well as the total neutron yield. Running the same capsule calculation with and without mix can determine the importance of mix on the simulated yield. In the literature¹⁴, a common way to infer the importance of mix on the yield is to take the ratio of the experimental yield divided by the simulation yield. For a clean calculation, this is “yield over clean” (or YOC). The analogous ratio for a mix calculation is “yield over mix” (or YOM). We show the YOM values for a number of Omega capsules shot by ourselves and others^{15,16,17,18,19,20} in Figure 4. All of these capsules have similar sizes (850 to 900 μm in diameter) and were driven by a 1 ns square pulse with 20 to 23 kJ of laser energy (see Bradley²¹ for additional details). The capsules are labeled by whether they filled with DD or DT gas and whether they have more or less than 6 atm of gas. Note that the YOM values all lie between 1.0 and 0.10, and for capsule shell thicknesses between 15 and 32 μm , the YOM values fall in the range of 0.10 to 0.47. The fact that we have YOM values near unity for the thinnest capsules is not surprising, since the yield is produced when the shock hits the center (so-called exploding pusher capsules). These capsules have mix only from Richtmeyer-

Meshkov (RM) instabilities when the implosion shock breaks out of the shell/gas interface. The plateau in YOM as the shell becomes thicker than 15 μm suggests that we are capturing part of the Rayleigh-Taylor (RT) mix when the outgoing shock is recompressed by the incoming shell. We will need to have lasers in RAGE to see how much yield is lost from imprinting. HYDRA simulations show that the inclusion of laser imprinting can reduce the yield by a factor of 2 to 2.5. This would raise our YOM range to 0.25 to ~ 1 . We also computed YOC values for many of these capsules, which are denoted by small black “x” symbols. The YOC values are typically a factor of two or more below the YOM value. The clean calculations show a trend of declining yield with increasing capsule thickness, which is consistent with other results in the literature¹⁴.

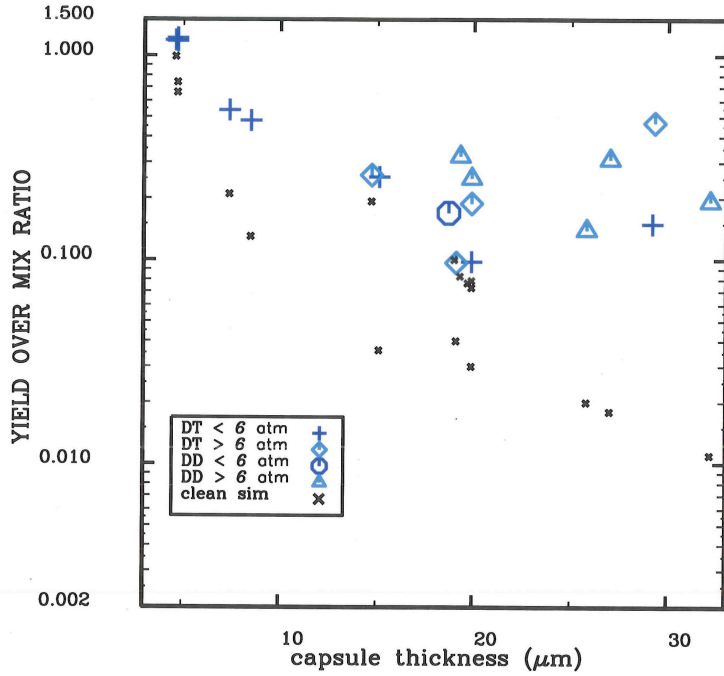


Figure 4: Yield over Mix (YOM) ratios for a variety of Omega capsules. The colored symbols represent YOM values for specific capsules. The small black “x” symbols are the analogous YOC values. The YOC and YOM values drop with increasing capsule thickness and reduced gas fill pressure, suggesting that BHR may not be mixing enough material at higher convergence ratios.

We also plotted the difference between the experimental²² and simulated burn averaged Tion value²¹, as shown in Figure 5. We use IDL²² scripts to postprocess the time dependent output information into DD, DT, or TT burn averaged ion temperatures. Thanks to improvements in the 3T modeling done early in 2013, the simulated Tion values are generally within 0.5 keV of the experimental values, which is generally the measurement error. There is one set of discrepant points. The thinnest shell ($<8.5 \mu\text{m}$) capsules have Tion values that are under-predicted by simulations, because the yield is produced solely when the shock hits the center. Eulerian codes tend to have problems adequately resolving converging shocks hitting a symmetry axis.

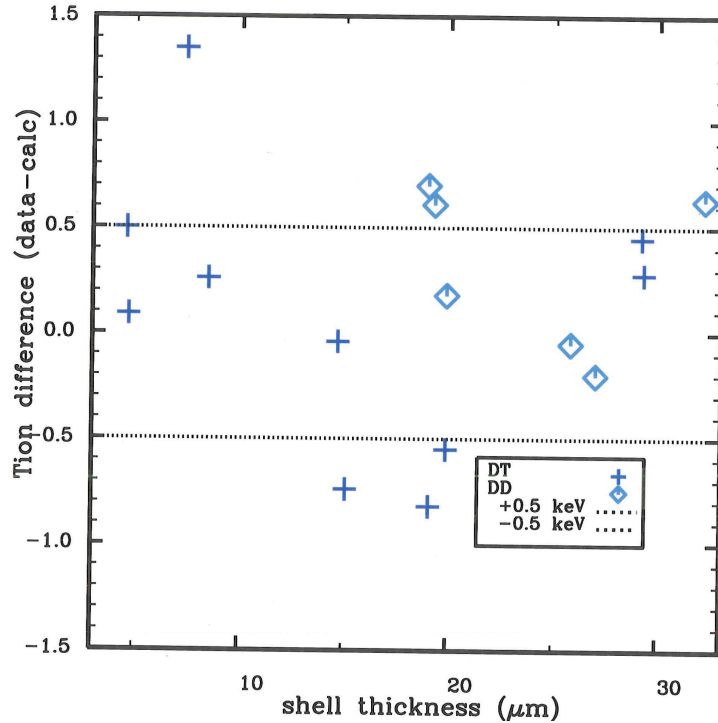


Figure 5: Burn averaged Tion differences (data-simulation) for the capsules shown in Figure 4. Almost all of the ΔTion values are less than 0.5 keV, which is roughly the measurement uncertainty.

We require our simulations to match the bang time by adjusting the width and energy of the source region to match both bang time and energy absorbed by the capsule (typically 60 to 65% of the incident energy¹⁰). We have two ways to compare our

simulations to the burn width. Most of our data consists of the full-width half-maximum (FWHM) burn width. In some cases, we have time-dependent burn history curves. In both cases, we take the time-dependent neutron yield rate from the simulation and convolve it with a Gaussian to mimic the diagnostic response (25 ps for DT and 50 ps for DD)²⁴. We have burn width ratios (data/simulation) for several DD and DT filled capsules with different thickness shells. The ratios are 1.8 to 1.9 for 8.5 μm thick CH shells and 1.6 to 1.7 for 15 μm thick shells. For DD capsules, we have ratios of 1.2 to 1.3 for 19 μm thick shells. Most of the improvement for the DD capsules comes from the 50 ps response function; if we use 25 ps, the ratio jumps up to 1.7 to 1.8. This discrepancy caused us to model the glass capsules reported in Herrmann et al.¹⁹ because they have time-dependent burn histories. The thin ($\sim 4 \mu\text{m}$) glass shell capsules produce most of their yield when the incoming shock hits the center. We show a plot of three simulated neutron burn histories from the DT reactions in Fig. 6. The simulated (full-width half-maximum) burn widths are within 10% of the data. The peak values are within 8% of the data; however when the experimental and simulated yields match, the simulated peak values are high. The YOM values are 1.22 to 1.18 for the three shots.

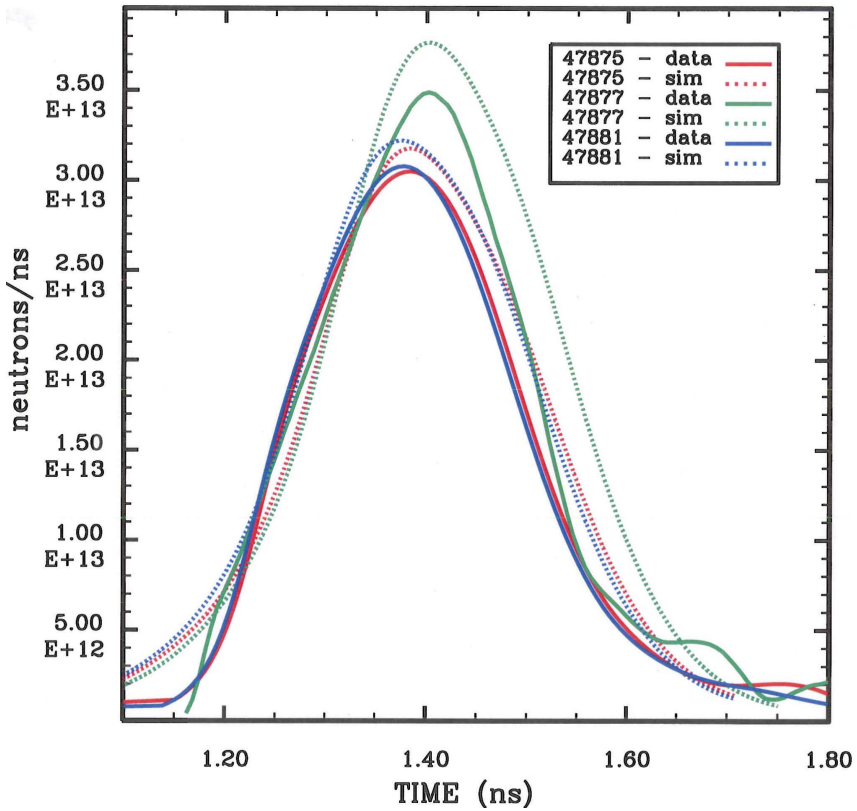


Figure 6: A plot of the neutron and gamma time history from a glass capsule with 5 atm DT gas (shot 47877)¹⁹. The simulation curves are shifted about 100 ps earlier to match the experimental bang time. The general shapes are similar, but the peak values and widths do not agree.

C. X-ray spectral diagnostics

The next category of data are spectroscopic measurements. Here, we have streak camera spectra that are time resolved but spatially integrated, and we have MMI data, which are spatially resolved, but limited to a few times. For both of these, we can create 1-D or 2-D maps of the electron temperature, electron density, and material composition that are combined with YORICK²⁵ scripts that include the details of the MMI x-ray mirrors, diagnostic mount, and filters. The first example we show is an Omega capsule with a Ti dopant layer next to the DD gas, as shown in Fig. 7. The simulation (right

panel) replicates the qualitative features of the data (left panel), but the line ratios do not match precisely. More work is needed with the mix models to provide a quantitative comparison to data. We are also able to produce synthetic MMI images, as shown in Fig. 8. The bright features of this image arise from the Ly- α line of Ti. The resultant spectrum is shown in Fig. 9 and is similar to the observed and synthetic spectra in Fig. 7. Although we can produce synthetic images, much more work is needed to extract physical quantities such as electron temperature maps that are needed to constrain models.

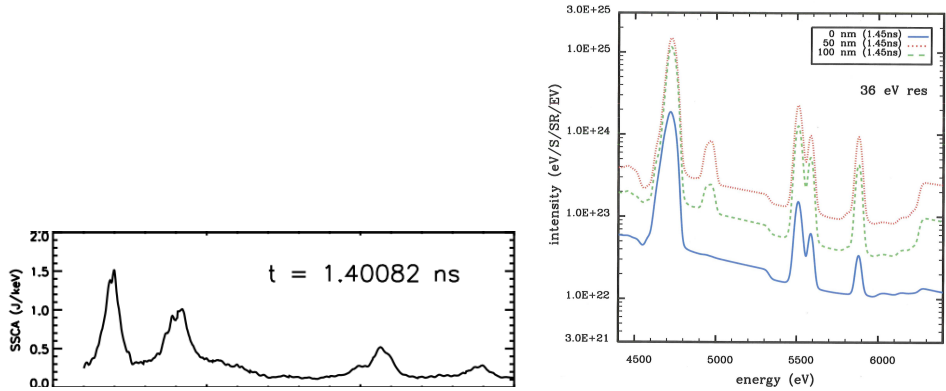


Figure 7: Sample spectra for an Omega capsule with a Ti dopant layer next to the gas (shot 65036). The left panel shows data from 1.45 ns. From left to right, the Ti He- α (4749 eV), Ly- α (4973 eV), He- β (5581 eV), and Ly- β + He- γ (5891+5873 eV) lines are clearly visible. The right panel shows the spectrum from a simulation with mix. The Ti lines are visible with mix, and the line strengths have the same qualitative trend as the data.

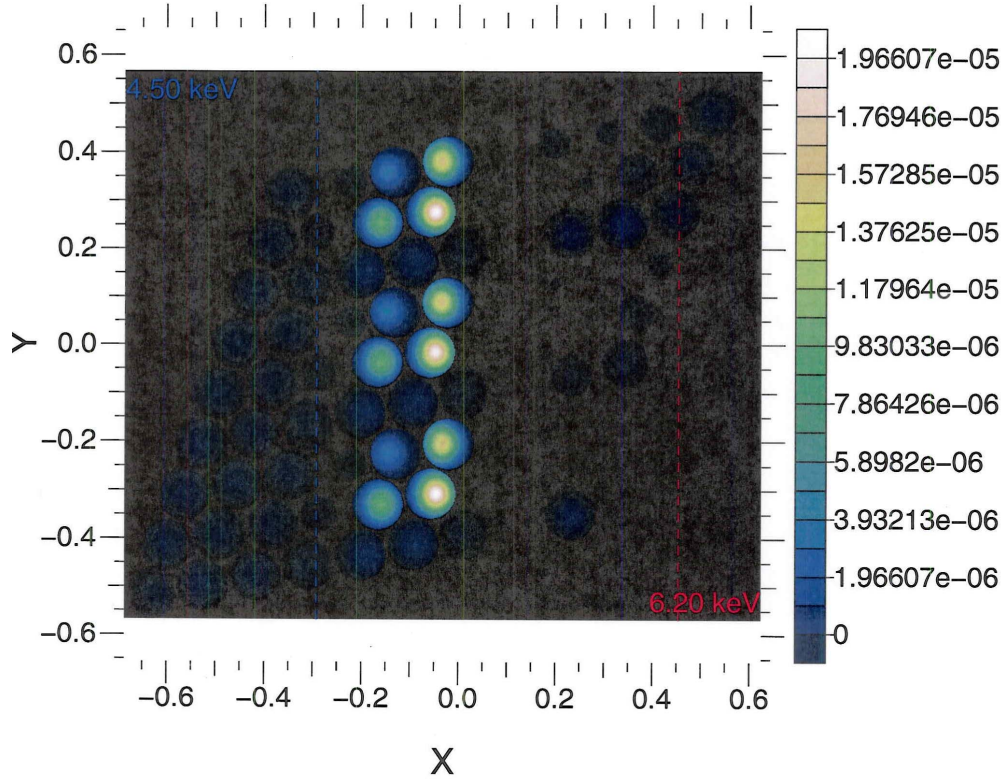


Figure 8: Sample image from the MMI simulator for Omega shot 65036 at 1.60 ns. The bright images running nearly vertically at -0.05 are caused by the Ti Ly- α line, while the fainter images to the left arise from the Ti He- α line.

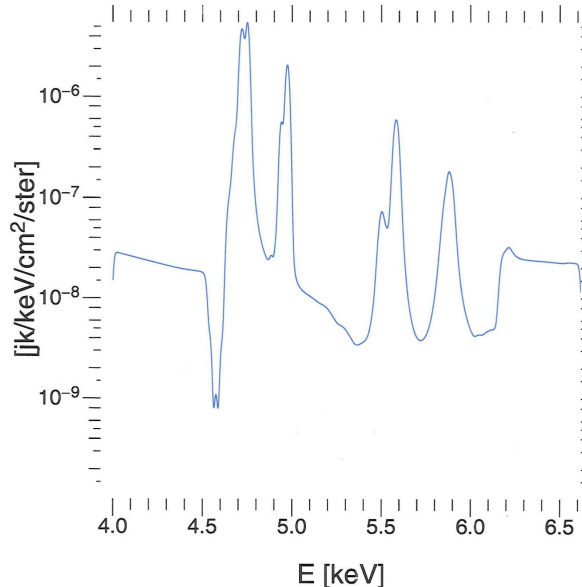


Figure 9: Sample synthetic spectrum for an Omega capsule with a Ti dopant layer next to the gas (shot 65036). This spectrum came from synthetic MMI images at 1.45 ns. The Ti He- α (4749 eV), Ly- α (4973 eV), He- β (5581 eV), and Ly- β + He- γ (5891+5873 eV) lines are clearly visible and are similar in intensity to the data in Figure 7.

D. Neutron imaging diagnostics

The final diagnostic we discuss is neutron imaging²⁶. Here, we take information from the RAGE run that can be read by the neutron-photon Monte-Carlo code MCNP²⁷ and post-processed to produce synthetic images for comparison to data. In Fig. 10, we show two images from a thin (42 μm) shell CD/T₂ capsule simulation during burn. The TT neutron image is in the left panel, while the DT neutron image is in the right panel. Both images are quite small, at 16 x 15 μm . More work is needed, preferably with National Ignition Campaign or CD Mixcap shots where there are neutron images that can be compared to simulations to ensure that the postprocessed image sizes are correct. For now, we note that the capability to produce these images exists.

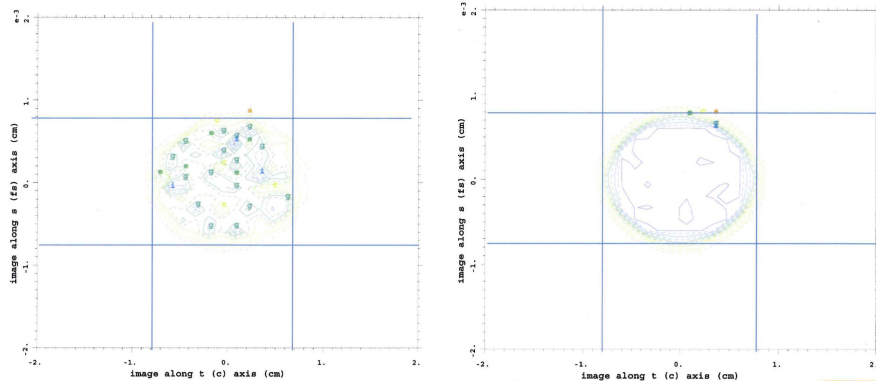


Figure 10: Sample neutron images from a NIF separated reactant capsule design.

The diameter is 2300 μm and the shell is 42 μm thick. The TT burn image is in the left panel, while the DT burn image is in the right panel. Both images are 16 x 15 μm across.

IV. Summary and Conclusions

Omega and NIF offer experimental platforms with a rich set of diagnostics. The DIME project is making use of these diagnostics to provide information about the mixing of material in plasma conditions and its effect on thermonuclear burn that can affect ignition. We are using RAGE as the code to model these experiments, but many synthetic diagnostics need to be constructed to allow for explicit comparisons of RAGE output to data from ICF experiments. We have shown comparisons to x-ray images, x-ray spectra, neutron yield, and neutron images that will provide valuable constraints on the mix model in RAGE.

Acknowledgements

The author wishes to thank L. Welser-Sherrill, Y.-H. Kim, and H. Herrmann for additional unpublished details from their experiments. We thank R. Rauenzahn and C. Wingate for help with code issues. We thank S. Batha and others for comments on this manuscript. This work was performed under the auspices of the U.S. Department of Energy by Los Alamos National Security, LLC under Contract No. DE-AC52-06NA25396.

REFERENCES

- 1 M. Gittings, R. Weaver, M. Clover, T. Betlach, N. Byrne, R. Coker, E. Dendy, R. Hueckstaedt, K. New, W.R. Oakes, D. Ranta, and R. Stefan, Computational Science and Discovery, **1**, 015005 (2008)
- 2 A. Banerjee, R.A. Gore, and M.J. Andrews, Phys. Rev. E, **82**, 046309, (2010)
- 3 J.D. Schwarzkopf, D. Livescu, R.A. Gore, R.M. Rauenzahn, J.R. Ristorcelli, Jour. Turbulence, **12**, 1 (2011)
- 4 G.R. Magelssen, J.A. Cobble, I.L Tregillis, M.J. Schmitt, S.H. Batha, P.A. Bradley,

and K.A. Defriend-Obrey, Journal of Physics, Conference Series, **244**, 022006 (2010)

5 P.A. Bradley, J.A. Cobble, I.L. Tregillis, M.J. Schmitt, K.D. Obrey, V. Glebov, S.H. Batha, G.R. Magelssen, J.R. Fincke, S.C. Hsu, N.S. Krasheninnikova, T.J. Murphy, and F.J. Wysocki, Phys. Plasmas, **19**, 092703 (2012)

6 J.A. Cobble, T.J. Murphy, M.J. Schmitt, P.A. Bradley, N.S. Krasheninnikova, K.A. Obrey, S.C. Hsu, I.L. Tregillis, G.R. Magelssen, F.J. Wysocki, and S.H. Batha, Phys. Plasmas, **19**, 122713 (2012)

7 M.J. Schmitt, P.A. Bradley, J.A. Cobble, J.R. Fincke, P. Hakel, S.C. Hsu, N.S. Krasheninnikova, G.A. Kyrala, G.R. Magelssen, D.S. Montgomery, T.J. Murphy, K.A. Obrey, R.C. Shah, I.L. Tregillis, J.A. Baumgaertel, F.J. Wysocki, S.H. Batha, R.S. Craxton, P.W. McKenty, P. Fitzsimmons, A. Nikroo, and R. Wallace, Phys. Plasmas, **20**, 056310 (2013)

8 T.R. Boehly, D. Brown, R. Craxton, R. Keck, J. Knauer, J. Kelly, T. Kessler, S. Kumpan, S. Loucks, S. Letzring, F. Marshall, R. McCrory, S. Morse, W. Seka, J. Soures, and C. Verdon, Opt. Commun. **133**, 495, (1997)

9 G.H. Miller, E.I. Moses, and C.R. Wuest, Nucl. Fusion, **44**, S228 (2004).

10 E.S. Dodd, J.F. Benage, G.A. Kyrala, D.C. Wilson, F.J. Wysocki, W. Seka, V. Yu. Glebov, C. Stoeckl, and J.A. Frenje, Phys. Plasmas, **19**, 042703 (2012)

11 J. Koch, T. Barbee, N. Izumi, R. Tommasini, R.C. Mancini, L.A. Welser, and F.J. Marshall, Rev. Sci. Instrum. **76**, 073708 (2005)

12 M.M. Marinak, G.D. Kerbel, N.A. Gentile, O. Jones, D. Munro, S. Pollaine, T.R. Dittrich, and S.W. Haan, Phys. Plasmas, **8**, 2275 (2001).

13 J.A. Oertel, T.N. Archuleta, and L.S. Shrake, Rev. Sci. Instrum. **72**, 701 (2001)

14 W.S. Varnum, N.D. Delamater, S.C. Evans, P.L. Gobby, J.E. Moore, J.M. Wallace, R.G. Watt, J.D. Colvin, R. Turner, V. Glebov, J. Soures, and C. Stoeckl, Phys. Rev. Letters, **84**, 5153 (2000)

15 L. Welser-Sherrill, J.H. Cooley, D.A. Haynes, D.C. Wilson, M.E. Sherrill, R.C. Mancini, and R. Tommasini, Phys. Plasmas, **15**, 072702 (2008)

16 P.B. Radha, J.A. Delettrez, R. Epstein, V. Yu Glebov, R. Keck, R.L. McCrory, P. McKenty, D.D. Meyerhofer, F. Marshall, S.P. Regan, S. Roberts, T.C. Sangster, W. Seka, S. Skupsky, V. Smalyuk, C. Sorce, C. Stoeckl, J. Soures, R.P.J. Town, B. Yaakobi, J. Frenje, C.K. Li, R. Petrasso, F. Seguin, K. Fletcher, S. Padalino, C. Freeman, N. Izumi, R. Lerche, and T.W. Phillips, Phys. Plasmas, **9**, 2208 (2002)

17 F.H. Seguin, C.K. Li, J.A. Frenje, D.G. Hicks, K.M. Green, S. Kurebayashi, R.D. Petrasso, J.M. Soures, D.D. Meyerhofer, V.Yu. Glebov, P.B. Radha, C. Stoeckl, S. Roberts, C. Sorce, T.C. Sangster, M.D. Cable, K. Fletcher, and S. Padalino, *Phys. Plasmas*, **9**, 2725 (2002)

18 C.K. Li, F.H. Seguin, D.G. Hicks, J.A. Frenje, K.M. Green, S. Kurebayashi, R.D. Petrasso, D.D. Meyerhofer, J.M. Soures, V.Yu. Glebov, R.L. Keck, P.B. Radha, S. Roberts, W. Seka, S. Skupsky, C. Stoeckl, and T.C. Sangster, *Phys. Plasmas*, **8**, 4902 (2001)

19 H.W. Herrmann, J.R. Langenbrunner, J.M. Mack, J.H. Cooley, D.C. Wilson, S.C. Evans, T.J. Sedillo, G.A. Kyrala, S.E. Caldwell, C.S. Young, A. Nobile, J. WErmer, S. Paglieri, A.M. McEvoy, Y. Kim, S.H. Batha, C.J. Horsfield, D. Drew, W. Garbett, M. Rubery, V.Yu. Glebov, S. Roberts, and J.A. Frenje, *Phys. Plasmas*, **16**, 056312 (2009)

20 Y.-H. Kim, and H.W. Herrmann, private communication (2014).

21 P.A. Bradley, “The Effect of Mix on Capsules Yields as a Function of Shell Thickness and Gas Fill”, *Phys. Plasmas*, submitted (2014)

22 T. J. Murphy, R. E. Chrien, and K. A. Klare, *Rev. Sci. Instr.*, **68**, 610 (1997)

23 ”Interactive Data Language User’s Guide”, Research Systems Inc., Boulder, CO, (1994)

24 R.A. Lerche, D.W. Phillion and G.L. Tietbohl, *Rev. Sci. Instr.*, **66**, 933, (1995)

25 D.H. Munro, *Comp. in Phys.* **9**, 609 (1995)

26 F.E. Merrill, D. Bower, R. Buckles, D.D. Clark, C.R. Danly, O.B. Drury, J.M. Dzenitis, V.E. Fatherley, D.N. Fittinghof, R. Gallegos, G.P. Grim, N. Guler, E.N. Loomis, S. Lutz, R.M. Malone, D.D. Martinson, D. Mares, D.J. Morley, G.L. Morgan, J.A. Oertel, I.L. Tregillis, P.L. Volegov, P.B. Weiss, C.H. Wilde, and D.C. Wilson, *Rev. Sci. Instr.*, **83**, 10D317, (2012)

27 “MCNP – A general Monte-Carlo N-particle Transport Code, Version 5”, April 24, 2003, X-5 Monte-Carlo team, LA-UR-03-1987

APPENDIX:

This appendix describes the post-processing programs and their locations. Our postprocessing tools are on hpss in /hpss/pbradley/TOOLS/OMEGA (or UOFI). These tools are subdivided into 1-D and 2-D versions in many cases. We list specific tools used for comparison to data below:

Backlit x-ray images: We can use opacities for a single representative condition and backlighter in each material in RAGE and create images. This can be done for multiple backlighters and opacity values. More recently, the capability was added to use the actual opacities on a point-by-point basis from the mesh given a particular backlighter energy. The backlit images can be postprocessed (typically take lineouts) to obtain radii for a given transmission level for a radius versus time plot.

Self-emission x-ray images: We have the RAGE dump reader file pio.f90 that extracts desired quantities from the mesh and writes them out in ASCII format. These files are read in by a code called spec3.f, which creates the requisite blackbody emission region surrounded by an absorbing shell. We use IDL scripts to create synthetic self-emission images for comparison to data.

Neutron yield, bang time, burn history, and burn width: We start by using grep to pull out all the lines with neutron (or gamma) burn information. We then use the code nalpha.f and galphaf to create files with the neutron (gamma) burn information that can be plotted and scaled to match data. The Los Alamos plot program POP has a Gaussian convolution function that we use to create instrumentally broadened burn history plots. The typical FWHM is 50 to 70 ps.

Burn averaged ion temperatures: We take RAGE HDF plots of Tion, DD, DT, and TT yields as function of time and space and process them with IDL scripts that produce DD, DT, or TT burn averaged temperatures. These scripts exist in 1-D and 2-D. Some versions of the scripts also compute averaged dopant region temperatures and ρr values as a function of time. A command card was recently installed in RAGE to compute DD or DT burn averaged Tion values directly from the run, which is being tested.

X-ray spectral diagnostics: We use pio.f90 to extract the needed information from 1-D or 2-D dumps files and then hand them off to Peter Hakel (1-D time dependent spectra) or Ian Tregillis (1-D or 2-D MMI plots and time dependent spectra).

Neutron imaging: We take special dump files produced by RAGE that can be read by MCNP and postprocessed to create neutron images. We use the same energy bins as the neutron imaging diagnostic at NIF to compare the images more directly. Further tools will be needed to convert the neutrons per pixel to the actual units of the neutron imager.

Mix mass: Although not measured, the data from experiments should constrain the mix mass. In 1-D, RAGE has the capability to write out the amount of material being mixed as a function of time. This capability does not exist in 2-D.